

# FDRMFL: Multi-modal Federated Feature Extraction Model Based on Information Maximization and Contrastive Learning

Haozhe Wu<sup>a</sup>

<sup>a</sup>*School of Computing and Data Science, The University of Hong Kong, Hong Kong SAR, China*

## ARTICLE INFO

### Keywords:

Multi-modal data analysis  
Feature extraction  
Federated learning  
Contrastive learning

## ABSTRACT

This study focuses on the feature extraction problem in multi-modal data regression. To address three core challenges in real-world scenarios: limited and non-IID data, effective extraction and fusion of multi-modal information, and susceptibility to catastrophic forgetting in model learning, a task-driven supervised multi-modal federated feature extraction method is proposed. The method integrates multi-modal information extraction and contrastive learning mechanisms, and can adapt to different neural network structures as the latent mapping functions for data of each modality. It supports each client to independently learn low-dimensional representations of multi-modal data, and can flexibly control the degree of retention of effective information about the response variable in the predictive variables within the low-dimensional features through parameter tuning. The multi-constraint learning framework constructed by the method guarantees regression accuracy using Mean Squared Error loss. Through the synergistic effect of mutual information preservation constraint, symmetric Kullback-Leibler divergence constraint, and inter-model contrastive constraint, it achieves the retention of task-related information, the extraction, fusion, and alignment of multi-modal features, and the mitigation of representation drift and catastrophic forgetting in non-IID scenarios, respectively. This ensures that the feature extraction process always centers on improving the performance of downstream regression tasks. Experimental results from simulations and real-world data analysis demonstrate that the proposed method achieves more significant performance improvement on downstream regression tasks compared with classical feature extraction techniques.

## 1. Introduction

With the continuous iteration of data acquisition technologies and the exponential growth of storage medium capacity, unstructured data such as images, audio, and text have exhibited an explosive growth trend, gradually becoming the core information carriers in the data-driven research paradigm [7]. Compared with traditional structured data, such unstructured data have essential differences in topological structure, and their inherent correlation patterns usually do not satisfy the linear structure assumption in Euclidean space, making it difficult for traditional Euclidean distance measurement methods to effectively model and represent them. Such data with complex structural characteristics are defined as multimodal data [23]. In many research fields, sample data based on non-Euclidean space have continuously emerged, posing fundamental challenges to traditional statistical analysis methods that rely on vector structures. Multimodal data have a wide range of application scenarios, and typical examples cover multiple disciplinary fields: phylogenetic tree structures in evolutionary biology [4], observation objects used for cell differentiation modeling in developmental biology, and probability distribution functions in nonlinear Wasserstein geometric space [25]; tensor data representing diffusion tensors and brain connection structures in neuroscience, and symmetric positive definite matrices on nonlinear Riemannian manifolds [1, 8, 28]; Laplacian operators used for graph structure analysis in network science [9], image, speech, text, and video data in social information fields [6], and data used for tumor shape modeling in medical

imaging [21]. For more application examples of multimodal data, please refer to relevant literature reviews [14].

In recent years, analytical methods for non-Euclidean modal data have gradually formed a system and achieved a series of progress in theoretical research and practical applications. For example, Faraway et al. [10] constructed a data model based on distance matrices; by predefining distance functions, they embedded data into low-dimensional Euclidean space for subsequent analysis using multidimensional scaling. Hein et al. [12] proposed a nonparametric kernel smoothing estimator for random variables in metric spaces. In terms of applications, multimodal data analysis has been used for graph-structure-driven image semantic segmentation and 3D point cloud target recognition in the field of computer vision; in the field of natural language processing, multimodal recognition technology has demonstrated excellent performance in semantic reasoning and cross-language text clustering tasks; in the field of speech processing, significant breakthroughs have been made in key issues such as speech emotion recognition based on manifold structure and robust speech feature selection [16, 26, 27, 20]. However, most existing methods have a key assumption: there is a fixed functional relationship between predictor variables and response variables in multimodal data analysis. This assumption is often difficult to hold in actual complex scenarios, which greatly limits the applicability and scalability of models in complex tasks. Compared with directly constructing the correlation between multimodal data and response variables of downstream tasks, realizing sufficient extraction and fusion of multimodal information under the premise of ensuring the performance accuracy of

\*Corresponding author. Email address: haozhe\_wu@connect.hku.hk

downstream tasks may be a more feasible research direction. At the same time, multimodal data usually face the problem of high acquisition difficulty, so how to effectively integrate data from multiple information sources has become a key scientific issue. As a collaborative training framework with "data not leaving the local end", federated learning realizes knowledge sharing while ensuring data privacy, providing an effective solution for multi-information source integration [22, 15]. However, when dealing with non-independent and identically distributed (non-IID) data, traditional federated learning models face prominent challenges such as representation drift and modal alignment difficulties [19, 3]. Especially in high-dimensional regression tasks, when the number of samples is limited but the feature dimension is extremely high, the curse of dimensionality further aggravates the instability of the model. Against this background, feature dimensionality reduction has become a core key issue in the field of federated multimodal learning. Traditional linear unsupervised dimensionality reduction techniques (such as Principal Component Analysis (PCA), Random Projection (RP), and Truncated Singular Value Decomposition (TSVD)) have been widely used in centralized scenarios, but they exhibit significant limitations in federated multimodal scenarios: First, PCA extracts principal components by maximizing variance, focusing on data reconstruction rather than predictive correlation, and it is easy to discard key feature directions with low variance but high correlation with target variables [2]; second, based on the Johnson–Lindenstrauss lemma, RP approximately preserves the distance between samples through random matrices, but there is a risk that key predictive signals are randomly discarded [5]; third, although TSVD can achieve low-rank compression [11], it completely ignores supervised labels and modal alignment information. These defects lead to problems such as performance fluctuations, generalization ability degradation, and low communication efficiency when such methods are directly applied to federated multimodal regression tasks. More importantly, these methods assume that data are centralized and identically distributed; in cross-client non-IID distribution scenarios, local feature subspaces will shift significantly, further damaging model consistency [17, 18]; at the same time, such unsupervised learning algorithms cannot guarantee the performance requirements of downstream tasks. It is worth noting that even Variational Autoencoders (VAE), a commonly used dimensionality-reduction approach for supervised prediction, face challenges in federated multimodal settings—their generative probabilistic modeling introduces extra computational burden, aligning latent spaces across clients is nontrivial, and the guidance for downstream prediction can be insufficient, making it difficult to preserve task-critical features precisely.[13]

In view of this, this paper aims to propose a novel multimodal feature extraction method under the federated learning framework. The core design of this method includes three key innovations: First, it uses an adaptive neural network structure to align each modal data to a latent vector space with fixed dimensions; it controls the effective information retention between multimodal features and response variables

through the mutual information maximization criterion, and uses KL divergence constraints to make the vector outputs of each mode as independent as possible, thereby reducing the negative impact of information redundancy. Second, it introduces a contrastive learning regularization mechanism: it pairs the local representation of the current round with the global representation of the previous round as positive samples, constructs a negative sample set with the global representations of earlier historical rounds, and adopts a contrastive loss in the form of InfoNCE to suppress client drift and alleviate catastrophic forgetting [24]. Third, it uses the flexible and powerful nonlinear fitting ability and implicit expression mechanism of neural networks to construct the correlation mapping between latent vector representations and response variables, and ensures the accuracy of downstream tasks based on the mean square expected risk minimization criterion. To verify the effectiveness of the proposed method, comparative experiments were carried out on three sets of simulated datasets and two sets of real near-infrared spectroscopy datasets. Experimental results show that the proposed method (FDRMFL) significantly outperforms traditional baseline methods such as PCA, RP, TSVD and MAE on all datasets, achieving lower mean square error. This result confirms that in federated multimodal regression tasks, the feature dimensionality reduction method integrating mutual information preservation, cross-modal alignment, and contrastive consistency constraints can effectively improve the predictive performance and stability of the model.

The subsequent structure of this paper is arranged as follows: Section 2 elaborates on the multimodal federated feature extraction model based on information maximization and contrastive learning and its parameter estimation method; Section 3 presents the analysis results of simulated experiments and real dataset experiments; Section 4 summarizes the full text and looks forward to future research directions.

## 2. Methodology

### 2.1. Multi-modal federated feature extraction

In the federated learning scenario, we consider a multimodal prediction problem involving  $K$  clients, where the local data distribution of the  $i$ -th client is  $P_i$ , and the weight of its samples in the global data is  $\pi_i$  (satisfying  $\sum_{i=1}^K \pi_i = 1$ ). Therefore, the overall distribution of the global data can be defined as  $P = \sum_{i=1}^K \pi_i P_i$ . The local data of each client contains multi-modal inputs  $X_i = (X_{i1}, X_{i2}, \dots, X_{iM})$ , where  $X_{im}$  represents the  $m$ -th modality data of the  $i$ -th client (such as text, image, time series, etc.). Different modalities correspond to dedicated neural network encoders: text data can be processed using Transformer to obtain features  $z_{i,\text{text}} = h_{\text{text}}(X_{i,\text{text}})$ , image data can be processed using GCNN to obtain features  $z_{i,\text{img}} = h_{\text{img}}(X_{i,\text{img}})$ , time series data can be processed using LSTM to obtain features  $z_{i,\text{seq}} = h_{\text{seq}}(X_{i,\text{seq}})$ , and so on. The dimensions of all modality features are unified to  $d$ . These modality features are mapped to a unified latent representation  $Z_i = g(z_{i1}, z_{i2}, \dots, z_{iM})$  through a fusion

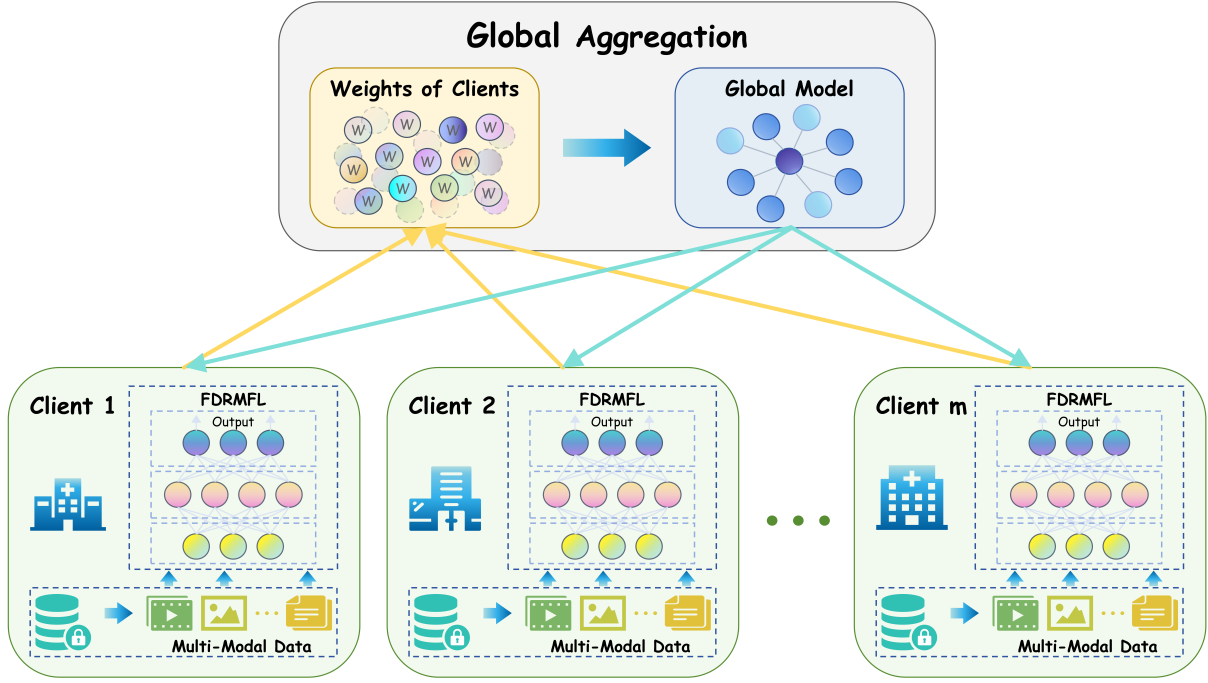


Fig. 1: Overall architecture for federated multi-modal learning.

function  $g$ . The final prediction output is given by  $f(Z_i)$ , and it satisfies the following relationship with the true labels:

$$y_i = f(Z_i) + \epsilon_i \quad (1)$$

where  $\epsilon_i$  is a random error term (satisfying  $\mathbb{E}[\epsilon_i|Z_i] = 0$  and  $\text{Var}(\epsilon_i|Z_i) = \sigma_{\epsilon,i}^2$ ). The optimization goal of the global model is to minimize the overall risk, which includes four terms: prediction loss, mutual information regularization, modality alignment regularization, and federated contrastive regularization, which are defined as follows. First, the prediction loss is used to measure the deviation between the model's predicted value and the true label, and is defined based on the expectation of the global distribution as:

$$\mathcal{L}_{\text{pred}} = \mathbb{E}_{(X_i, y_i) \sim P} [(y_i - f(Z_i))^2] \quad (2)$$

Since  $y_i = f(Z_i) + \epsilon_i$ , this equation can be expanded as

$$\mathbb{E}[\epsilon_i^2] = \sum_{i=1}^K \pi_i \left( \sigma_{\epsilon,i}^2 + \mathbb{E}[(f(Z_i) - \mathbb{E}[y_i|Z_i])^2|P_i] \right), \quad (3)$$

which includes both the weighted variance of the random errors of each client and the deviation between the prediction function and the conditional expectation, ensuring the basic prediction capability of the model.

Secondly, there is a mutual information regularization term, which aims to maximize the mutual information between the latent representation  $Z_i$  and the label  $y_i$  to ensure

that  $Z_i$  contains sufficient predictive information. The mutual information  $I(Z_i; y_i)$  is defined as:

$$I(Z_i; y_i) = \mathbb{E}_{P(Z_i, y_i)} \log \frac{P(Z_i, y_i)}{P(Z_i)P(y_i)} \quad (4)$$

It is equivalent to  $H(y_i) - H(y_i|Z_i)$  (where  $H(\cdot)$  is the entropy), so the regularization term can be written as

$$\mathcal{R}_{\text{mi}} = -I(Z_i; y_i) \quad (5)$$

By Jensen's inequality, the mutual information can also be expressed as

$$\mathbb{E}_{P(y_i)} \mathbb{E}_{P(Z_i|y_i)} \log \frac{P(Z_i|y_i)}{P(Z_i)} \quad (6)$$

This form reveals the conditional dependence of  $Z_i$  on  $y_i$  - the more information  $Z_i$  contains about  $y_i$ , the greater the difference between the conditional distribution  $P(Z_i|y_i)$  and the marginal distribution  $P(Z_i)$ , and the greater the mutual information.

The third term is a modal alignment regularization, which is used to minimize the difference between the feature distributions of different modalities, ensuring the consistency of multi-modal fusion. For any two modalities  $m$  and  $n$  of the  $i$ -th client, the symmetric KL divergence is used to measure the distance between their feature distributions  $p(z_{im})$  and

$p(z_{in})$ :

$$\text{symKL}(p(z_{im}), p(z_{in})) = \frac{1}{2} \left( \text{KL}(p(z_{im}) \| p(z_{in})) + \text{KL}(p(z_{in}) \| p(z_{im})) \right) \quad (7)$$

where the KL divergence is defined as:

$$\text{KL}(p \| q) = \mathbb{E}_p \log \frac{p(z)}{q(z)} \quad (8)$$

After averaging over all modal pairs, combined with the expectation of the global distribution, the regularization term is defined as:

$$\mathcal{R}_{kl} = \mathbb{E}_{(X_i, y_i) \sim P} \left[ \frac{1}{\binom{M}{2}} \sum_{1 \leq m < n \leq M} \text{symKL}(p(z_{im}), p(z_{in})) \right] \quad (9)$$

If we assume that the features of each modality follow a homoscedastic Gaussian distribution

$$p(z_{im}) \sim \mathcal{N}(\mu_{im}, \sigma^2 I) \text{ and } p(z_{in}) \sim \mathcal{N}(\mu_{in}, \sigma^2 I) \quad (10)$$

Then the KL divergence can be simplified to

$$\text{KL}(\mathcal{N}(\mu_{im}, \sigma^2 I) \| \mathcal{N}(\mu_{in}, \sigma^2 I)) = \frac{1}{2\sigma^2} \|\mu_{im} - \mu_{in}\|^2 \quad (11)$$

At this point, the symmetric KL divergence degenerates to  $\frac{1}{2\sigma^2} \|\mu_{im} - \mu_{in}\|^2$ , which intuitively reflects the difference between the mean vectors of the two modal features.

Finally, the federated contrastive regularization, aiming at the problem that the local update of the client in federated learning may deviate from the global model, uses the InfoNCE form to constrain the consistency between the current representation and the historical global representation. Let  $Z_i$  be the representation output by the current model of the  $i$ -th client,  $Z_{i,\text{prev}}^g$  be the representation of the same input  $X_i$  by the global model of the previous round (positive sample), and  $\{Z_{i,\text{hist}}^g\}$  be the set of representations of earlier global models (negative samples), then the regularization term is defined as:

$$\mathcal{R}_{fcl} = \mathbb{E}_{(X_i, y_i) \sim P} \left[ -\log \frac{\exp(\text{sim}(Z_i, Z_{i,\text{prev}}^g)/\tau)}{\exp(\text{sim}(Z_i, Z_{i,\text{prev}}^g)/\tau) + \sum_{z \in \{Z_{i,\text{hist}}^g\}} \exp(\text{sim}(Z_i, z)/\tau)} \right] \quad (12)$$

where  $\text{sim}(a, b) = \frac{a^\top b}{\|a\| \|b\|}$  is the cosine similarity, and  $\tau > 0$  is the temperature coefficient. This formula maximizes the similarity between the current representation and the positive sample and minimizes the similarity with the negative samples, forcing the local model update to maintain consistency with the global model.

Combining the above four items, the global overall risk is:

$$\mathcal{L}_{\text{total}} = \mathcal{L}_{\text{pred}} + \lambda_1 \mathcal{R}_{mi} + \lambda_2 \mathcal{R}_{kl} + \lambda_3 \mathcal{R}_{fcl} \quad (13)$$

where  $\lambda_1, \lambda_2, \lambda_3 > 0$  are regularization coefficients, which are used to balance the influence of each term.

## 2.2. Estimations of model

In actual training, sample estimation is used to replace the overall expectation. For the  $i$ -th client, given a local batch sample  $\mathcal{B}_i = \{(X_{i1}, y_{i1}), (X_{i2}, y_{i2}), \dots, (X_{ib}, y_{ib})\}$  ( $b$  is the batch size), the empirical prediction loss is:

$$\mathcal{L}_{\text{pred},i}^{\text{emp}} = \frac{1}{b} \sum_{j=1}^b (y_{ij} - f(Z_{ij}))^2 \quad (14)$$

where  $Z_{ij} = g(z_{ij1}, z_{ij2}, \dots, z_{ijM})$  is the fused representation of the  $j$ -th sample for the  $i$ -th client, and  $z_{ijm} = h_m(X_{ijm})$  is its  $m$ -th modal feature.

The estimation of empirical mutual information can be achieved through variational lower bound: Since  $I(Z_{ij}; y_{ij}) \geq \mathbb{E}[\log \sigma(f(Z_{ij}) \cdot y_{ij}) + \log(1 - \sigma(f(Z_{ij}) \cdot \tilde{y}_{ij}))]$  (where  $\tilde{y}_{ij}$  is the negative sample label, and  $\sigma$  is the sigmoid function), the empirical mutual information regularization term for the  $i$ -th client is:

$$\mathcal{R}_{mi,i}^{\text{emp}} = -\frac{1}{b} \sum_{j=1}^b \left[ \log \sigma(f(Z_{ij}) \cdot y_{ij}) + \log(1 - \sigma(f(Z_{ij}) \cdot \tilde{y}_{ij})) \right] \quad (15)$$

The empirical modal alignment loss averages the symmetric KL divergence calculated for each sample's modal feature pairs in the batch:

$$\mathcal{R}_{kl,i}^{\text{emp}} = \frac{1}{\binom{M}{2}} \sum_{1 \leq m < n \leq M} \frac{1}{b} \sum_{j=1}^b \text{symKL}(z_{ijm}, z_{ijn}). \quad (16)$$

Under a Gaussian approximation, this reduces to

$$\mathcal{R}_{kl,i}^{\text{emp}} \approx \frac{1}{2b\sigma^2 \binom{M}{2}} \sum_{1 \leq m < n \leq M} \sum_{j=1}^b \|z_{ijm} - z_{ijn}\|^2. \quad (17)$$

The empirical federated contrastive loss is:

$$\mathcal{R}_{fcl,i}^{\text{emp}} = \frac{1}{b} \sum_{j=1}^b \mathcal{L}_{ij}^{\text{fcl}}. \quad (18)$$

The single-sample loss is defined as

$$\mathcal{L}_{ij}^{\text{fcl}} = -\log \frac{\exp(\text{sim}(Z_{ij}, Z_{i,\text{prev}}^g)/\tau)}{\exp(\text{sim}(Z_{ij}, Z_{i,\text{prev}}^g)/\tau) + \sum_{z \in \mathcal{H}_i} \exp(\text{sim}(Z_{ij}, z)/\tau)} \quad (19)$$

where  $Z_{i,\text{prev}}^g$  is the representation of  $X_{ij}$  from the previous round's global model, and  $\mathcal{H}_i$  is the set of historical global representations stored by the  $i$ -th client.

Finally, the empirical overall risk for the  $i$ -th client is:

$$\mathcal{L}_{\text{empirical},i} = \mathcal{L}_{\text{pred},i}^{\text{emp}} + \lambda_1 \mathcal{R}_{mi,i}^{\text{emp}} + \lambda_2 \mathcal{R}_{kl,i}^{\text{emp}} + \lambda_3 \mathcal{R}_{fcl,i}^{\text{emp}} \quad (20)$$

The model training process follows the federated learning framework: the server initializes the global parameters  $w^0 = \{h_1^0, h_2^0, \dots, h_M^0, g^0, f^0\}$ , and distributes the parameters  $w^t$  to all clients in each round; the  $i$ -th client calculates the gradient of the empirical loss  $\mathcal{L}_{\text{empirical},i}$  based on the local data and parameters  $w^t$ , and updates the local parameters through gradient descent  $w_i^t \leftarrow w_i^t - \eta \nabla \mathcal{L}_{\text{empirical},i}$  ( $\eta$  is the learning

rate); after  $E$  rounds of local iteration, the client returns the updated parameters  $w_i^{t,E}$ , and the server aggregates the new global parameters by weighting by the number of samples:

$$w^{t+1} = \sum_{i=1}^K \frac{|D_i|}{\sum_{j=1}^K |D_j|} w_i^{t,E} \quad (21)$$

where  $|D_i|$  is the total number of samples for the  $i$ -th client. Through multiple rounds of iteration, the global model is gradually optimized, and finally achieves accurate prediction and representation alignment in a multi-modal federated scenario. We refer to the above model as the Multi-modal Federated Feature Extraction Model Based on Information Maximization and Contrastive Learning (FDRMFL), and its computational process under limited samples is shown in Algorithm 1.

Building upon FedAvg training and standard alignment losses, we introduce a communication-stage synergy of cross-modal KL alignment and contrastive learning to jointly enforce cross-modal consistency and cross-client stability. We further adopt coordinated weight scheduling to mitigate forgetting/drift and stability strategies tailored to non-IID small samples. While FedAvg and basic alignment losses are prior art, our contribution lies in the combined constraints and stabilization that are particularly suitable for federated multimodal regression.

---

**Algorithm 1** Multi-modal Federated Feature Extraction Model Based on Information Maximization and Contrastive Learning (FDRMFL)

---

```

1: Server initializes global model parameters  $w^0 = \{h_1^0, h_2^0, \dots, h_M^0, g^0, f^0\}$ .
2: for  $t = 0, \dots, T - 1$  do
3:   Broadcasts the global parameters  $w^t$  to all  $K$  clients.
4:   for each client  $i = 1, 2, \dots, K$  in parallel do
5:     Initializes local parameters  $w_i^t \leftarrow w^t$ .
6:     for local epoch  $e = 1, \dots, E$  do
7:       Samples a mini-batch  $B_i = \{(X_{ij}, y_{ij})\}_{j=1}^b$  from local dataset  $D_i$ .
8:       Computes modal features  $z_{ijm} = h_m(X_{ijm})$  for  $m = 1, \dots, M$  and
         fusion representation  $Z_{ij} = g(z_{ij1}, \dots, z_{ijM})$ .
9:       Computes previous global representation
          $Z_{ij,prev}^s = g^t(h_1^t(X_{ij1}), \dots, h_M^t(X_{ijM}))$ .
10:      Calculates empirical losses:
11:       $\mathcal{L}_{pred,i}^{emp}, \mathcal{R}_{mi,i}^{emp}, \mathcal{R}_{kl,i}^{emp}, \mathcal{R}_{fcl,i}^{emp}$ .
12:      Computes total empirical loss:
13:       $\mathcal{L}_{empirical,i} = \mathcal{L}_{pred,i}^{emp} + \lambda_1 \mathcal{R}_{mi,i}^{emp} + \lambda_2 \mathcal{R}_{kl,i}^{emp} + \lambda_3 \mathcal{R}_{fcl,i}^{emp}$ .
14:      Updates local parameters via gradient descent:
15:       $w_i^t \leftarrow w_i^t - \eta \nabla \mathcal{L}_{empirical,i}$ .
16:    end for
17:    Sends the updated local parameters  $w_i^{t,E}$  to the server.
18:  end for
19:  Server aggregates parameters by sample size weighting:
     $w^{t+1} = \sum_{i=1}^K \frac{|D_i|}{\sum_{j=1}^K |D_j|} w_i^{t,E}$ .
20: end for
21: Outputs the final global model.
```

---

### 2.3. The global parameter settings of FDRMFL

In the multi-modal Federated Feature Extraction Model (FDRMFL), the core components of the global parameter  $w^t = \{h_1^t, h_2^t, \dots, h_M^t, g^t, f^t\}$  can be divided into two main parts: one part is the parameter set of the neural network  $f$  used for the final prediction, and the other part is the

parameter set of the dedicated encoders  $h_1, h_2, \dots, h_M$  corresponding to  $M$  different modalities of data. The parameters of the fusion function  $g$  are also included in the global parameters, which together constitute the core parameter system for model training and updating. From a mathematical expression perspective, the update process of the global parameters follows the federated averaging rule, that is, the new global parameters aggregated by the server after each iteration are:

$$w^{t+1} = \sum_{i=1}^K \frac{|D_i|}{\sum_{j=1}^K |D_j|} w_i^{t,E} \quad (22)$$

where  $|D_i|$  is the number of samples of the  $i$ -th client, and  $w_i^{t,E}$  is the parameter of the client after  $E$  rounds of local iterations. For text, image, time series, and common vector-valued data, the model uses Transformer, CNN, LSTM, and multi-layer neural networks as dedicated encoders, respectively. The parameters of these encoders and the parameters of the prediction network  $f$  together constitute the core content of the global parameters. The following will elaborate on the specific composition of  $w$  in detail, combined with the mathematical principles and key formulas of the neural networks corresponding to each modality. For the Transformer encoder  $h_{\text{text}}$  for text data, its core mathematical principle is based on the self-attention mechanism and the stacking of encoder layers. Its parameters include multi-head self-attention layer parameters, feedforward neural network layer parameters, and layer normalization parameters. The text data is first subjected to word embedding and position encoding to obtain the input matrix  $X_{\text{text}} \in \mathbb{R}^{n \times d_{\text{model}}}$  ( $n$  is the sequence length, and  $d_{\text{model}}$  is the model dimension). The self-attention mechanism obtains the query vector  $Q$ , the key vector  $K$ , and the value vector  $V$  by performing linear transformations on the input matrix, so as to capture the semantic association of different positions in the text sequence. The linear transformation formula is:

$$Q = X_{\text{text}} W_Q \quad (23)$$

$$K = X_{\text{text}} W_K \quad (24)$$

$$V = X_{\text{text}} W_V \quad (25)$$

where  $W_Q, W_K, W_V \in \mathbb{R}^{d_{\text{model}} \times d_k}$  are the query, key, and value matrices ( $d_k$  is the dimension of the attention head), which are the core learnable parameters of the self-attention layer. The attention score is calculated by the dot product of  $Q$  and  $K$  transpose, scaled, and then normalized by the Softmax function to obtain the attention weight. The formula is:

$$\text{Attention}(Q, K, V) = \text{Softmax}\left(\frac{QK^T}{\sqrt{d_k}}\right)V \quad (26)$$

Multi-head self-attention divides  $Q, K, V$  into  $h$  heads and calculates attention scores in parallel. Then, the results of multiple heads are fused by the concatenation matrix  $W_O$  to realize the capture of associations in different semantic dimensions. The specific formula is:

$$\text{MultiHead}(Q, K, V) = \text{Concat}(\text{head}_1, \text{head}_2, \dots, \text{head}_h) W_O \quad (27)$$



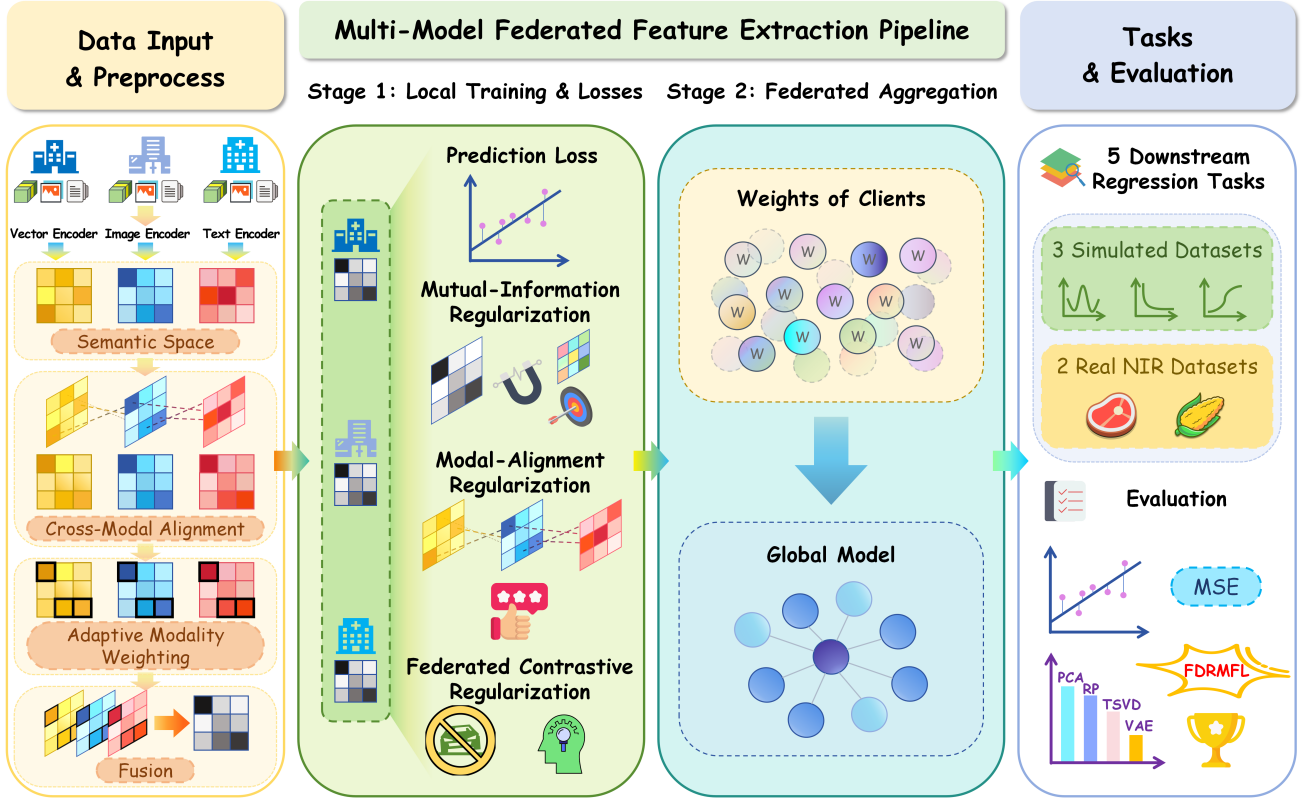


Fig. 2: FDRMFL Multi-Model Federated Feature Extraction and Evaluation Pipeline

where

$$\text{head}_i = \text{Attention}(QW_{Q_i}, KW_{K_i}, VW_{V_i}), \quad i = 1, \dots, h,$$

and  $W_{Q_i}, W_{K_i}, W_{V_i} \in \mathbb{R}^{d_{\text{model}} \times d_k}$  are the linear transformation matrices of the  $i$ -th attention head, while  $W_O \in \mathbb{R}^{hd_k \times d_{\text{model}}}$  is the output projection matrix; all of them are learnable parameters.

$$\text{FFN}(x) = \max(0, xW_1 + b_1)W_2 + b_2 \quad (28)$$

where  $W_1 \in \mathbb{R}^{d_{\text{model}} \times d_{\text{ff}}}$  and  $W_2 \in \mathbb{R}^{d_{\text{ff}} \times d_{\text{model}}}$  are the weight matrices ( $d_{\text{ff}}$  is the hidden layer dimension of the feedforward network), and  $b_1 \in \mathbb{R}^{d_{\text{ff}}}$  and  $b_2 \in \mathbb{R}^{d_{\text{model}}}$  are the bias vectors. At the same time, layer normalization (Layer Normalization) is used in the encoder layer to stabilize the training process. The formula is:

$$\text{LayerNorm}(x) = \gamma \cdot \frac{x - \mathbb{E}[x]}{\sqrt{\text{Var}(x) + \epsilon}} + \beta \quad (29)$$

where  $\gamma \in \mathbb{R}^{d_{\text{model}}}$  and  $\beta \in \mathbb{R}^{d_{\text{model}}}$  are the scaling factor and offset factor, respectively, which are the learnable parameters of layer normalization, and  $\epsilon$  is a small constant to prevent the denominator from being zero. These parameters of the multi-head self-attention layer, feedforward neural network layer, and layer normalization together constitute the component of the Transformer encoder in the global parameters.

The CNN encoder  $h_{\text{img}}$  for image data is based on the combination of convolution operations, pooling operations,

and fully connected layers. Its parameters mainly include convolution kernel weights, biases, and fully connected layer weights and biases. The input image data is typically a three-dimensional tensor  $X \in \mathbb{R}^{H \times W \times C_{\text{in}}}$  ( $H$  is the height,  $W$  is the width, and  $C_{\text{in}}$  is the number of input channels). The convolution operation achieves feature extraction through the sliding dot product of a two-dimensional convolution kernel and local image features. The calculation of the  $k$ -th output feature map is:

$$Z_k = \sum_{c=1}^{C_{\text{in}}} X_c * K_{k,c} + b_k \quad (30)$$

where  $K_{k,c} \in \mathbb{R}^{k_h \times k_w}$  is the convolution kernel weight of the  $k$ -th output channel corresponding to the  $c$ -th input channel ( $k_h$  and  $k_w$  are the height and width of the convolution kernel, respectively),  $b_k \in \mathbb{R}$  is the corresponding bias, and  $*$  represents the two-dimensional convolution operation, whose specific discrete form is:

$$(X_c * K_{k,c})(i, j) = \sum_{p=0}^{k_h-1} \sum_{q=0}^{k_w-1} X_c(i+p, j+q) K_{k,c}(p, q) \quad (31)$$

After the convolution operation, an activation function is usually connected to introduce non-linearity. A commonly used ReLU activation function is:

$$a_k(i, j) = \max(0, Z_k(i, j)) \quad (32)$$

Subsequently, a pooling operation is performed to reduce the feature dimension. Taking max pooling as an example, its calculation is:

$$\text{MaxPool}(a_k)(i, j) = \max_{p \in [iS, (i+1)S-1]} \max_{q \in [jS, (j+1)S-1]} a_k(p, q) \quad (33)$$

where  $S$  is the pooling stride, and the pooling layer has no learnable parameters. After multiple rounds of convolution and pooling, the feature map is flattened into a one-dimensional vector  $X_{\text{flat}} \in \mathbb{R}^{d_{\text{flat}}}$  ( $d_{\text{flat}}$  is the flattened dimension), which is input to the fully connected layer. The calculation of the fully connected layer is:

$$Z_{\text{fc}} = X_{\text{flat}} W_{\text{fc}} + b_{\text{fc}} \quad (34)$$

$$a_{\text{fc}} = \max(0, Z_{\text{fc}}) \quad (35)$$

where  $W_{\text{fc}} \in \mathbb{R}^{d_{\text{flat}} \times d_{\text{fc}}}$  and  $b_{\text{fc}} \in \mathbb{R}^{d_{\text{fc}}}$  are the weight matrix and bias vector of the fully connected layer, respectively ( $d_{\text{fc}}$  is the output dimension of the fully connected layer). Finally, the feature is mapped to a modal feature of a unified dimension  $d$  through the output layer:

$$z_{\text{img}} = a_{\text{fc}} W_{\text{out}} + b_{\text{out}} \quad (36)$$

where  $W_{\text{out}} \in \mathbb{R}^{d_{\text{fc}} \times d}$  and  $b_{\text{out}} \in \mathbb{R}^d$  are the weight matrix and bias vector of the output layer. These convolution kernel weights  $K_{k,c}$ , convolution biases  $b_k$ , fully connected layer weights  $W_{\text{fc}}$ ,  $W_{\text{out}}$  and biases  $b_{\text{fc}}$ ,  $b_{\text{out}}$  together constitute the parameter set of the CNN encoder.

The LSTM encoder  $h_{\text{seq}}$  for processing time-series data addresses long-sequence dependencies through a gating mechanism. Its parameters include weight matrices and bias vectors for the input gate, forget gate, cell gate, and output gate. The time-series input is  $x_t \in \mathbb{R}^{d_{\text{in}}}$  (where  $t$  is the time step and  $d_{\text{in}}$  is the input dimension), and the core states of the LSTM are the cell state  $C_t \in \mathbb{R}^{d_h}$  and the hidden state  $h_t \in \mathbb{R}^{d_h}$  (where  $d_h$  is the hidden layer dimension). The calculations for each gate are based on the concatenated vector  $[h_{t-1}, x_t] \in \mathbb{R}^{d_h+d_{\text{in}}}$  of the current input  $x_t$  and the previous hidden state  $h_{t-1}$ . First, the forget gate is calculated to control the retention ratio of the previous cell state:

$$f_t = \sigma(W_f[h_{t-1}, x_t] + b_f) \quad (37)$$

where  $W_f \in \mathbb{R}^{d_h \times (d_h+d_{\text{in}})}$  is the weight matrix of the forget gate,  $b_f \in \mathbb{R}^{d_h}$  is the bias vector of the forget gate, and  $\sigma(x) = \frac{1}{1+e^{-x}}$  is the sigmoid activation function, with an output range between  $[0, 1]$ . Values closer to 1 indicate more retention of previous state information. Next, the input gate and cell candidate state are calculated, jointly determining the incorporation of new information:

$$i_t = \sigma(W_i[h_{t-1}, x_t] + b_i) \quad (38)$$

$$\tilde{C}_t = \tanh(W_C[h_{t-1}, x_t] + b_C) \quad (39)$$

where  $W_i \in \mathbb{R}^{d_h \times (d_h+d_{\text{in}})}$  and  $W_C \in \mathbb{R}^{d_h \times (d_h+d_{\text{in}})}$  are the weight matrices for the input gate and cell candidate

state, respectively, and  $b_i \in \mathbb{R}^{d_h}$  and  $b_C \in \mathbb{R}^{d_h}$  are the corresponding bias vectors.  $\tanh(x) = \frac{e^x - e^{-x}}{e^x + e^{-x}}$  is the hyperbolic tangent function, with an output range between  $[-1, 1]$ . The cell state is updated through the collaborative action of the forget gate and input gate:

$$C_t = f_t \odot C_{t-1} + i_t \odot \tilde{C}_t \quad (40)$$

where  $\odot$  denotes element-wise multiplication. Finally, the output gate is calculated to control the output of the cell state to the hidden state:

$$o_t = \sigma(W_o[h_{t-1}, x_t] + b_o) \quad (41)$$

$$h_t = o_t \odot \tanh(C_t) \quad (42)$$

where  $W_o \in \mathbb{R}^{d_h \times (d_h+d_{\text{in}})}$  is the weight matrix of the output gate, and  $b_o \in \mathbb{R}^{d_h}$  is the bias vector of the output gate. To obtain modal features with a uniform dimension  $d$ , a linear layer needs to be connected after the LSTM output:

$$z_{\text{seq}} = h_T W_{\text{lstm-out}} + b_{\text{lstm-out}} \quad (43)$$

where  $h_T$  is the hidden state of the last time step of the sequence, and  $W_{\text{lstm-out}} \in \mathbb{R}^{d_h \times d}$  and  $b_{\text{lstm-out}} \in \mathbb{R}^d$  are the weight matrix and bias vector of the linear layer. These gate weight matrices  $W_f, W_i, W_C, W_o$ , gate bias vectors  $b_f, b_i, b_C, b_o$ , and output linear layer parameters  $W_{\text{lstm-out}}, b_{\text{lstm-out}}$  collectively constitute the core parameters of the LSTM encoder.

For a multi-layer neural network encoder  $h_{\text{vec}}$  designed for common vector-valued data, its mathematical principle is based on the stacking of fully connected layers and the nonlinear mapping of activation functions, with the parameters being the weight matrices and bias vectors of each layer. The vector-valued input is  $X_{\text{vec}} \in \mathbb{R}^{d_{\text{in}}}$  ( $d_{\text{in}}$  is the input dimension). Assuming the network contains  $L$  hidden layers, each layer achieves feature extraction through a combination of linear transformation and nonlinear activation. The calculation process for the first hidden layer is:

$$z_1 = W_1 X_{\text{vec}} + b_1 \quad (44)$$

$$a_1 = \sigma(z_1) \quad (45)$$

where  $W_1 \in \mathbb{R}^{d_1 \times d_{\text{in}}}$  is the weight matrix of the first hidden layer ( $d_1$  is the output dimension of the first hidden layer),  $b_1 \in \mathbb{R}^{d_1}$  is the bias vector of the first hidden layer, and  $\sigma$  is the activation function, commonly the ReLU function  $\sigma(x) = \max(0, x)$  or the sigmoid function  $\sigma(x) = \frac{1}{1+e^{-x}}$ . For the  $l$ -th ( $2 \leq l \leq L$ ) hidden layer, its input is the output of the previous hidden layer  $a_{l-1} \in \mathbb{R}^{d_{l-1}}$ , and the calculation process is:

$$z_l = W_l a_{l-1} + b_l \quad (46)$$

$$a_l = \sigma(z_l) \quad (47)$$

where  $W_l \in \mathbb{R}^{d_l \times d_{l-1}}$  is the weight matrix of the  $l$ -th hidden layer,  $b_l \in \mathbb{R}^{d_l}$  is the bias vector of the  $l$ -th hidden layer, and  $d_l$  is the output dimension of the  $l$ -th hidden layer. To unify the modal features to dimension  $d$ , an output layer is set at

the end of the network to map the output of the  $L$ -th hidden layer  $a_L \in \mathbb{R}^{d_L}$  to the target dimension:

$$z_{\text{vec}} = W_{L+1}a_L + b_{L+1} \quad (48)$$

where  $W_{L+1} \in \mathbb{R}^{d \times d_L}$  is the weight matrix of the output layer, and  $b_{L+1} \in \mathbb{R}^d$  is the bias vector of the output layer. The weight matrices  $W_1, W_2, \dots, W_L$ , the bias vectors  $b_1, b_2, \dots, b_L$  of each hidden layer, as well as the weight matrix  $W_{L+1}$  and the bias vector  $b_{L+1}$  of the output layer together constitute the parameter set of the multi-layer neural network encoder, and these parameters are updated through the backpropagation algorithm based on the gradient of the loss function.

The neural network  $f$  used for the final prediction has a parameter structure similar to that of a multi-layer neural network. The core is to use a fully connected layer to perform nonlinear mapping on the fused unified latent representation  $Z_i \in \mathbb{R}^d$  ( $d$  is the dimension of the fused feature) to output the predicted value. The parameters include the weight matrix and bias vector of each fully connected layer. Assuming that the prediction network contains  $L_f$  hidden layers and the input is  $Z_i$ , the calculation of the first hidden layer is:

$$z_{f,1} = W_{f,1}Z_i + b_{f,1} \quad (49)$$

$$a_{f,1} = \sigma(z_{f,1}) \quad (50)$$

where  $W_{f,1} \in \mathbb{R}^{d_{f,1} \times d}$  is the weight matrix of the first hidden layer ( $d_{f,1}$  is the output dimension of the first hidden layer),  $b_{f,1} \in \mathbb{R}^{d_{f,1}}$  is the bias vector of the first hidden layer, and  $\sigma$  is the activation function. For the  $l$ -th ( $2 \leq l \leq L_f$ ) hidden layer, the input is the output of the previous hidden layer  $a_{f,l-1} \in \mathbb{R}^{d_{f,l-1}}$ , and the calculation process is:

$$z_{f,l} = W_{f,l}a_{f,l-1} + b_{f,l} \quad (51)$$

$$a_{f,l} = \sigma(z_{f,l}) \quad (52)$$

where  $W_{f,l} \in \mathbb{R}^{d_{f,l} \times d_{f,l-1}}$  is the weight matrix of the  $l$ -th hidden layer,  $b_{f,l} \in \mathbb{R}^{d_{f,l}}$  is the bias vector of the  $l$ -th hidden layer, and  $d_{f,l}$  is the output dimension of the  $l$ -th hidden layer. According to the prediction task type (regression or classification), the output layer adopts different calculation methods: if it is a regression task, the output layer directly outputs continuous values:

$$y_{\text{pred}} = W_{f,L_f+1}a_{f,L_f} + b_{f,L_f+1} \quad (53)$$

If it is a classification task, the output layer needs to be connected to the Softmax function to obtain the class probability:

$$y_{\text{pred}} = \text{Softmax}(W_{f,L_f+1}a_{f,L_f} + b_{f,L_f+1}) \quad (54)$$

where  $\text{Softmax}(x)_k = \frac{e^{x_k}}{\sum_{m=1}^C e^{x_m}}$  ( $C$  is the number of classes),  $W_{f,L_f+1} \in \mathbb{R}^{C \times d_{f,L_f}}$  (classification task) or  $W_{f,L_f+1} \in \mathbb{R}^{1 \times d_{f,L_f}}$  (regression task) is the weight matrix of the output layer, and  $b_{f,L_f+1} \in \mathbb{R}^C$  (classification task) or  $b_{f,L_f+1} \in \mathbb{R}$

(regression task) is the bias vector of the output layer. In addition, if the fusion function  $g$  is implemented using a neural network, taking attention fusion as an example, its calculation process is as follows: first, calculate the attention weights of each modality feature:

$$\alpha_m = \frac{e^{z_m W_{\text{att}}}}{\sum_{n=1}^M e^{z_n W_{\text{att}}}} \quad (55)$$

Then, obtain the fusion feature by weighted summation:

$$Z_i = \sum_{m=1}^M \alpha_m z_m W_{\text{fusion}} + b_{\text{fusion}} \quad (56)$$

where  $W_{\text{att}} \in \mathbb{R}^{d \times 1}$  is the attention weight calculation matrix,  $W_{\text{fusion}} \in \mathbb{R}^{d \times d}$  is the fusion weight matrix, and  $b_{\text{fusion}} \in \mathbb{R}^d$  is the fusion bias vector. These parameters are also included in the global parameter  $w$ , and together with the encoder parameters of each modality and the prediction network parameters, constitute a complete global parameter system.

### 3. Data analysis

#### 3.1. Simulation studies

To evaluate, in a controlled setting, the robustness and predictive accuracy of the proposed FDRMFL framework under different data and federated configurations, we construct tri-modal synthetic data and compare against classic dimensionality-reduction baselines. For data generation, three modalities are adopted: an image tensor of shape  $(N, 3, 32, 32)$ , a text tensor of shape  $(N, 10, 50)$ , and a vector modality of shape  $(N, 32)$ . To obtain reusable and interpretable cross-modal statistics, each sample's three modalities are first flattened; we then perform stride-10 subsampling and summation to obtain three scalar statistics. A weighted combination of these statistics is subsequently passed through different nonlinear transformations to produce the target variable. Concretely, the first link function augments the weighted sum with a weak interaction term—the product of the image and text statistics with a tiny weight—and then applies a softplus transform, yielding positive, monotonically increasing outputs; the second link function applies a hyperbolic tangent transform directly to the weighted sum, compressing outputs into a symmetric bounded interval; the third link function also builds on the weighted sum but uses a symmetric bounded hyperbolic transform whose shape is equivalent to a hyperbolic-secant curve, which can be viewed as a constant numerator divided by the sum of the positive and negative exponentials of the signal, peaking near zero and rapidly decaying towards both tails.

To avoid notational ambiguity, we now present the formal definitions of the three link functions. Let the flattened vectors for the  $i$ -th sample be  $\text{vec}(\text{img}^{(i)}) \in \mathbb{R}^{D_{\text{img}}}$ ,  $\text{vec}(\text{txt}^{(i)}) \in \mathbb{R}^{D_{\text{txt}}}$ , and  $\text{vec}^{(i)} \in \mathbb{R}^{D_{\text{vec}}}$ , and define

$$J(D) = \{1, 11, 21, \dots\} \cap \{1, \dots, D\}, \quad (57)$$

$$s_{\text{img}}^{(i)} = \sum_{j \in J(D_{\text{img}})} (\text{vec}(\text{img}^{(i)}))_j, \quad s_{\text{txt}}^{(i)} = \sum_{j \in J(D_{\text{txt}})} (\text{vec}(\text{txt}^{(i)}))_j, \quad s_{\text{vec}}^{(i)} = \sum_{j \in J(D_{\text{vec}})} (\text{vec}^{(i)})_j. \quad (58)$$



On this basis, the three link functions are written as

$$y^{(i)} = \log\left(1 + \exp\left(0.1 s_{\text{img}}^{(i)} + 0.1 s_{\text{txt}}^{(i)} + 0.1 s_{\text{vec}}^{(i)} + 10^{-4} s_{\text{img}}^{(i)} s_{\text{txt}}^{(i)}\right)\right) \quad (59)$$

$$y^{(i)} = \tanh\left(0.05 s_{\text{img}}^{(i)} + 0.05 s_{\text{txt}}^{(i)} + 0.05 s_{\text{vec}}^{(i)}\right) \quad (60)$$

$$y^{(i)} = \frac{16}{\exp\left(0.02 s_{\text{img}}^{(i)} + 0.02 s_{\text{txt}}^{(i)} + 0.02 s_{\text{vec}}^{(i)}\right) + \exp\left(-0.02 s_{\text{img}}^{(i)} - 0.02 s_{\text{txt}}^{(i)} - 0.02 s_{\text{vec}}^{(i)}\right)} \quad (61)$$

Samples are then randomly partitioned across three clients; the training set contains 2000 examples and the test set contains 500 examples. After shuffling indices, clients randomly draw to form local train/test splits and participate in federated training. The above procedure is kept identical across multiple repeated runs so that stability can be assessed under different link-function and client combinations.

For the experimental setup, each client contains dedicated encoders for the three modalities: a convolutional network for images, a bidirectional LSTM for text, and a multilayer perceptron for vectors. The three encoded outputs are aligned and aggregated in a fusion layer to obtain a unified multi-modal representation, which is regressed to a scalar output. Federated training adopts a standard configuration (e.g., 5 federation rounds, 3 local epochs per client, batch size 32, Adam with learning rate 0.001). The compared methods are listed by name only: PCA, TSVD, RP, MAE and the proposed FDRMFL. The sole evaluation metric is the mean squared error (MSE). For each scenario we perform multiple repeated runs and report the statistics of MSE; subsequent comparisons are made solely on the means reported in the table. Unless otherwise noted, all tables report mean (std) over  $N=10$  runs; boldface indicates the best in column.

Results are shown in Table 1 and Figure 3. Across the nine sub-scenarios formed by the three link functions and three clients, FDRMFL attains the lowest MSE in 9/9 cases. Averaged over all sub-scenarios, the mean MSEs are: PCA 0.817, TSVD 0.839, RP 0.825, and FDRMFL 0.541, so relative to the best overall baseline (PCA, 0.817), FDRMFL achieves an average relative reduction of about 33.8%.

Examining the three link functions separately, the largest gains occur under the more challenging Link-1 regime. In Link-1, the best baseline is PCA with an average MSE of 1.478, while FDRMFL averages 0.901, corresponding to an absolute reduction of about 0.577 and a relative reduction of about 39.1%. In Link-2, the best groupwise baseline is again PCA (0.452) versus FDRMFL (0.337), giving an absolute reduction of about 0.115 and a relative reduction of about 25.4%. In Link-3, the best baseline is RP (0.519) versus FDRMFL (0.386), yielding an absolute reduction of about 0.133 and a relative reduction of about 25.6%. At the sub-scenario level, the relative reduction versus the best baseline in that sub-scenario ranges from approximately 19.1% to 45.2% (lowest at Link-3, client 2; highest at Link-1, client 1). Representative examples include Link-1 with client 3, where FDRMFL achieves 0.8125 (0.0763) compared with PCA 1.2305 (0.1143), TSVD 1.1680 (0.0993), and RP 1.1666 (0.1037); Link-2 with client 1, where FDRMFL attains 0.3191 (0.0166) versus PCA 0.4174 (0.0273), TSVD

0.4626 (0.0235), and RP 0.4785 (0.0257); and Link-3 with client 1, where FDRMFL is 0.3596 (0.0219) compared with PCA 0.4711 (0.0354), TSVD 0.4921 (0.0225), and RP 0.4594 (0.0249).

Overall, these results show that FDRMFL provides consistently lower MSEs than the linear dimensionality-reduction baselines across all link functions and client partitions. The absolute gaps are larger in the higher-MSE Link-1 regime, while in the relatively lower-MSE Link-2 and Link-3 regimes the advantage remains stable and evident, indicating that the proposed constraints improve predictive performance in both difficult and relatively easier settings.

To further strengthen the baseline comparison, we additionally include a standard VAE trained under exactly the same data generation, task, and evaluation protocol as the original experiments, using the latent mean as input to the downstream regression model. As shown in Table 2 and Figure 4, FDRMFL attains lower test MSE than VAE in all 9 settings across 3 link functions  $\times$  3 clients. The relative MSE reduction ranges from 22.31% to 65.84%, with an overall average of 42.96%; when aggregated by link function, the average reductions are 41.83% for Link Function 1, 33.09% for Link Function 2, and 53.96% for Link Function 3.

These results indicate that, even when compared with a nonlinear generative model, FDRMFL learns representations that are more stable and more tightly aligned with the regression targets in the non-IID, small-sample federated multimodal setting. In particular, the explicitly task-driven mutual-information, cross-modal alignment, and contrastive-consistency constraints provide a stronger inductive bias toward predictive features than the unsupervised reconstruction objective used by VAE.

### 3.2. Real data analysis

To verify the effectiveness of the proposed method, this paper conducts experiments using two types of classic public benchmark datasets in the field of near-infrared spectroscopy, both of which have broad academic recognition. The first is the meat dataset, derived from the Carnegie Mellon University Statistics Library (<http://lib.stat.cmu.edu/datasets/tecator>), which is a benchmark public dataset for functional data modeling and regression prediction research in the field of near-infrared spectroscopy analysis. This dataset contains 240 meat samples without missing values, and each sample contains two parts of information: one is 3 scalar chemical components (moisture, fat, protein); the other is a near-infrared absorption spectrum curve  $X(t)$ , with a band range of 850–1050 nm, collected at 2 nm intervals, for a total of 101 wavelength points, belonging to the functional covariate of the  $L^2(T)$  space. In the experimental design, the near-infrared absorption spectrum curve is used as the functional mode, two of the 3 scalar chemical components are selected as the vector mode, and the remaining one is used as the prediction target  $Y$ . Three sets of experiments are constructed by successively rotating them to verify the effectiveness of the algorithm in the bimodal scene. The second is the corn dataset, derived from the Eigenvector Research Institute public library

**Table 1**  
MSE comparison of methods under Link Function scenarios

Link Function	Client ID	PCA	TSVD	RP	FDRMFL
Link-1	1	1.6768(0.1569)	1.7938(0.1744)	1.7144(0.1668)	<b>0.9193(0.0844)</b>
	2	1.5276(0.1427)	1.5381(0.1402)	1.5770(0.1373)	<b>0.9708(0.0741)</b>
	3	1.2305(0.1143)	1.1680(0.0993)	1.1666(0.1037)	<b>0.8125(0.0763)</b>
Link-2	1	0.4174(0.0273)	0.4626(0.0235)	0.4785(0.0257)	<b>0.3191(0.0166)</b>
	2	0.4336(0.0238)	0.4777(0.0305)	0.4342(0.0325)	<b>0.3483(0.0178)</b>
	3	0.5054(0.0315)	0.4531(0.0205)	0.4950(0.0375)	<b>0.3442(0.0224)</b>
Link-3	1	0.4711(0.0354)	0.4921(0.0225)	0.4594(0.0249)	<b>0.3596(0.0219)</b>
	2	0.4958(0.0286)	0.5304(0.0281)	0.5566(0.0344)	<b>0.4013(0.0223)</b>
	3	0.5986(0.0244)	0.6371(0.0492)	0.5414(0.0275)	<b>0.3971(0.0152)</b>

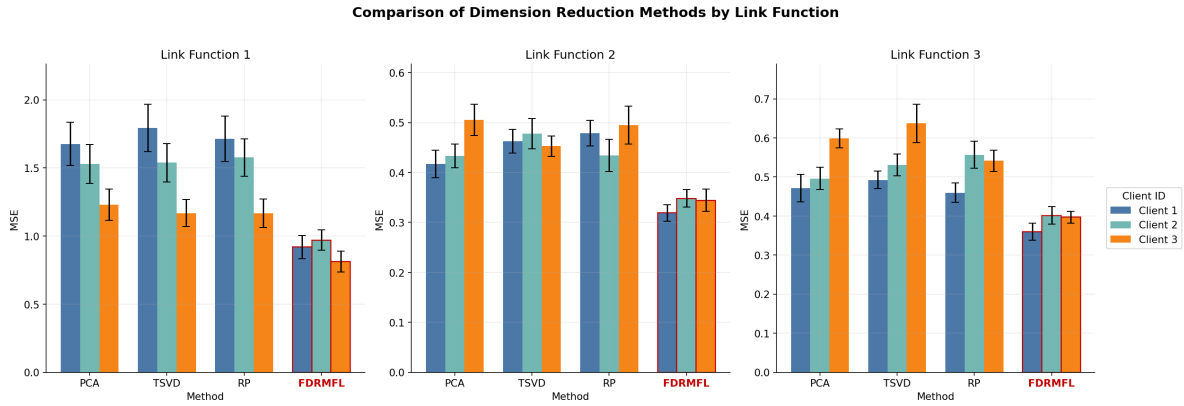


**Fig. 3:** Visualization of the MSE comparison of methods under Link Function scenarios

(<http://eigenvector.com/data/corn/index.html>), which is a typical dataset for grain composition prediction research in the field of agricultural chemistry. This dataset contains 80 corn samples, and each sample also contains two parts of information: one is 4 scalar chemical components (oil content, moisture, starch, protein); the other is a near-infrared absorption spectrum curve  $X(t)$ , with a band range of 1100–2498 nm, collected at 2 nm intervals, for a total of 700 wavelength points, also belonging to the functional covariate of the  $L^2(T)$  space. The experimental design is consistent

with the meat dataset: the near-infrared absorption spectrum curve is used as the functional mode, three of the 4 scalar chemical components are selected as the vector mode, and the remaining one is used as the prediction target  $Y$ . Four sets of experiments are constructed by successively rotating them to further verify the algorithm's bimodal adaptation capability. The experiment uses mean square error (MSE) as the core evaluation index. Unless otherwise specified, the training process of all models is performed after each round of global aggregation, and the MSE is calculated and

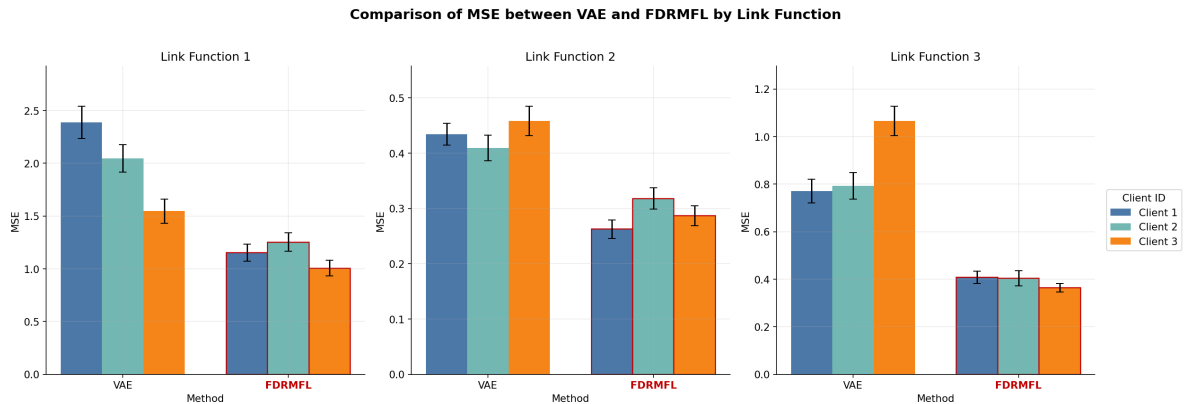


**Fig. 4:** Visualization of the MSE comparison between VAE and FDRMFL under different link functions

**Table 2**

Comparison of MSE of VAE and FDRMFL in different link functions

Link Function	Client ID	VAE	FDRMFL
Link-1	1	2.3882(0.1536)	<b>1.1526(0.0818)</b>
	2	2.0473(0.1307)	<b>1.2535(0.0868)</b>
	3	1.5461(0.1135)	<b>1.0052(0.0737)</b>
Link-2	1	0.4342(0.0198)	<b>0.2627(0.0167)</b>
	2	0.4096(0.0234)	<b>0.3182(0.0190)</b>
	3	0.4583(0.0268)	<b>0.2866(0.0180)</b>
Link-3	1	0.7705(0.0504)	<b>0.4082(0.0253)</b>
	2	0.7924(0.0567)	<b>0.4040(0.0324)</b>
	3	1.0659(0.0618)	<b>0.3641(0.0180)</b>

recorded on the global test set, which is used as a comparison basis between different methods and configurations. To ensure the fairness of the evaluation, all comparison methods adopt the unified process of "intra-modal dimensionality reduction → downstream regression" to construct baseline models, and strictly maintain the same training/evaluation process, data division method, and random seeds on the two types of datasets, effectively avoiding evaluation bias. This paper selects principal component analysis (PCA), random projection (Random Projection), and truncated singular value decomposition (Truncated SVD) as comparison methods.

Dataset 1 concerns three response variables (protein, fat, moisture) measured on meat samples from three clients, where the near-infrared spectra are strongly corrupted by surface-texture noise and the client distributions differ markedly (for example, client 1 contains mostly lean samples, whereas client 3 contains mostly fatty samples). As shown in Table 3 and Figure 5, FDRMFL attains the lowest MSE for every target–client combination, and the performance margins over the baselines are even larger than in the simulation study.

For protein prediction, linear reductions such as PCA and TSVD, which emphasize global variance, fail to prioritize protein-relevant absorption bands (e.g., the amide region around 1000–1050 nm). By leveraging mutual-information regularization, FDRMFL drives the encoder toward task-relevant features and reduces the MSE to 0.3579/0.3313/0.1989 on clients 1/2/3, corresponding to an average gain of 36.5% over the best baseline. At the same time, the cross-client spread of FDRMFL (0.159) is substantially smaller than that of PCA (0.2695), indicating improved robustness to client heterogeneity.

For fat prediction, where the C–H vibration near 930 nm overlaps with moisture-related peaks, the cross-modal alignment term helps disentangle these signals. FDRMFL achieves MSEs of 0.1057/0.1444/0.1328 on clients 1/2/3, a 35.1%–66.8% relative improvement over the strongest baseline on each client, together with noticeably reduced inter-client gaps. For moisture prediction, whose spectral response is highly nonlinear (e.g., reflectance saturation at high moisture levels), FDRMFL maintains MSE values within the narrow range 0.2871–0.3189 across all clients,

which is 20.3% lower than the best baseline (0.3601) and still achieves the lowest error on client 3, where the underlying distribution is widest.

Overall, these results show that, on noisy and highly heterogeneous meat spectra, FDRMFL not only improves accuracy for all three targets but also yields more stable performance across clients, suggesting that the proposed constraints effectively mitigate the combined effects of surface-texture noise and non-IID client distributions.

Dataset 2 uses corn samples with four response variables (starch, protein, oil, moisture) measured over a longer wavelength range (1100–2498 nm). Spectral–chemical relations are more complex than in Dataset 1: overlaps around 1700 nm (starch C–O vs. oil C–H) complicate band attribution, and varietal differences introduce pronounced non-IID effects across clients. As shown in Table 4 and Figure 6, FDRMFL is overall more accurate and more stable than the baselines across all four targets.

For starch, where the spectral response is relatively weak and relies on peaks in the 1200–1300 nm band, the combination of mutual-information retention and cross-modal alignment helps localize weak peaks and suppress interference. FDRMFL achieves MSEs of 0.3970/0.5973/0.2291 on clients 1/2/3, representing a 16.4% drop relative to RP on client 2 and yielding a value on client 3 that is 0.653× that of TSVD.

For protein, which exhibits strong inter-variety shifts across clients, FDRMFL keeps the MSE within the range 0.2455–0.6014. On client 3, its MSE (0.6014) is 36.6% lower than PCA (0.9480), and on client 2, its MSE (0.2455) is 37.8% lower than RP (0.3951), thus achieving both high accuracy and reduced cross-client fluctuation.

For oil, whose spectral response is strongly nonlinear and particularly unsuitable for linear dimensionality reduction (e.g., TSVD reaches 0.8504 on client 3), FDRMFL attains 0.5367/0.2578/0.4657 on clients 1/2/3. This corresponds to a 45.2% reduction relative to TSVD on client 3, and FDRMFL is the only method that keeps the oil MSE below 0.6 for all clients.

For moisture, where baseline methods show substantial instability across clients, FDRMFL maintains MSEs within the narrow interval 0.1011–0.1244. The value for client 3 (0.1011) is the lowest among all methods and differs from client 1 (0.1244) by only 0.0233, making FDRMFL the only method with MSE < 0.13 on every client.

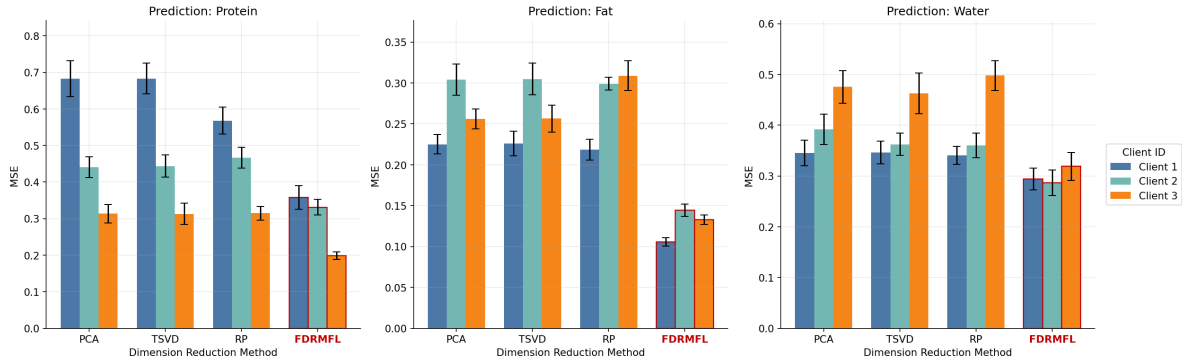
Together with the results on Dataset 1, these findings indicate that, under challenging corn spectra with overlapping bands and strong varietal heterogeneity, FDRMFL not only improves predictive accuracy for all targets but also substantially reduces performance variability across clients.

Mechanistically, mutual-information retention tightly couples the reduced representation with the target, prioritizing task-relevant spectral bands; cross-modal KL alignment calibrates and disentangles spectra with overlapping peaks (e.g., 930 nm, 1700 nm) using scalar/vector covariates; and federated contrastive consistency provides stable anchors across communication rounds, curbing representation drift and mitigating forgetting. In concert, these components

**Table 3**

Comparison of MSE of various methods in the scenarios of protein, fat and moisture prediction

Prediction Target	Client ID	PCA	TSVD	RP	FDRMFL
Protein	1	0.6827(0.0493)	0.6830(0.0418)	0.5676(0.0368)	<b>0.3579(0.0327)</b>
	2	0.4411(0.0286)	0.4437(0.0303)	0.4661(0.0285)	<b>0.3313(0.0208)</b>
	3	0.3134(0.0254)	0.3130(0.0291)	0.3146(0.0193)	<b>0.1989(0.0105)</b>
Fat	1	0.2251(0.0118)	0.2259(0.0151)	0.2183(0.0127)	<b>0.1057(0.0051)</b>
	2	0.3042(0.0192)	0.3049(0.0193)	0.2991(0.0080)	<b>0.1444(0.0076)</b>
	3	0.2560(0.0120)	0.2564(0.0163)	0.3089(0.0184)	<b>0.1328(0.0060)</b>
Water	1	0.3453(0.0255)	0.3460(0.0223)	0.3405(0.0175)	<b>0.2943(0.0214)</b>
	2	0.3921(0.0301)	0.3625(0.0219)	0.3601(0.0240)	<b>0.2871(0.0252)</b>
	3	0.4756(0.0323)	0.4630(0.0401)	0.4978(0.0294)	<b>0.3189(0.0277)</b>

**Fig. 5:** Visualization of the comparison of prediction MSE by various methods on the Tecator dataset

yield lower errors and smaller cross-client variance under high noise, peak overlap, strong non-IID, and nonlinearity, consistent with the advantages observed in Tables 3, 4 and the corresponding figures.

Across both real-world datasets, the findings closely mirror the simulation results, corroborating the generality and effectiveness of FDRMFL. First, task-driven feature retention (via mutual-information constraints) consistently prioritizes

target-relevant spectral bands, avoiding the “reduction-for-reduction’s-sake” losses seen in baselines. Second, cross-client representation stability (via contrastive consistency) effectively suppresses client drift under distribution shifts, yielding smaller MSE dispersion than competing methods. Third, multi-modal association adaptation (via cross-modal alignment) handles nonlinearity and overlapping spectral signals where linear reductions and single-modal designs fall short. In the comparative bar plots for both datasets (see

**Table 4**

Comparison of MSE of each method under the scenarios of starch, protein, fat, oil, and moisture content prediction

Prediction Target	Client ID	PCA	TSVD	RP	FDRMFL
Starch	1	0.4308(0.0313)	0.4508(0.0257)	0.5061(0.0298)	<b>0.3970(0.0328)</b>
	2	0.8341(0.0404)	0.8141(0.0578)	0.7144(0.0403)	<b>0.5973(0.0417)</b>
	3	0.3108(0.0258)	0.3508(0.0273)	0.3209(0.0271)	<b>0.2291(0.0131)</b>
Protein	1	0.5579(0.0449)	0.5379(0.0300)	0.5650(0.0307)	<b>0.4095(0.0306)</b>
	2	0.4930(0.0381)	0.4630(0.0256)	0.3951(0.0221)	<b>0.2455(0.0164)</b>
	3	0.9480(0.0832)	0.9280(0.0786)	0.8977(0.0675)	<b>0.6014(0.0477)</b>
Oil	1	0.6713(0.0422)	0.6763(0.0496)	0.7645(0.0535)	<b>0.5367(0.0467)</b>
	2	0.3911(0.0250)	0.3511(0.0308)	0.3757(0.0293)	<b>0.2578(0.0225)</b>
	3	0.8004(0.0529)	0.8504(0.0422)	0.8218(0.0691)	<b>0.4657(0.0337)</b>
Moisture	1	0.2166(0.0117)	0.1486(0.0059)	0.2326(0.0118)	<b>0.1244(0.0065)</b>
	2	0.1572(0.0086)	0.1783(0.0093)	0.1873(0.0099)	<b>0.1098(0.0040)</b>
	3	0.1229(0.0061)	0.1837(0.0081)	0.1361(0.0077)	<b>0.1011(0.0049)</b>

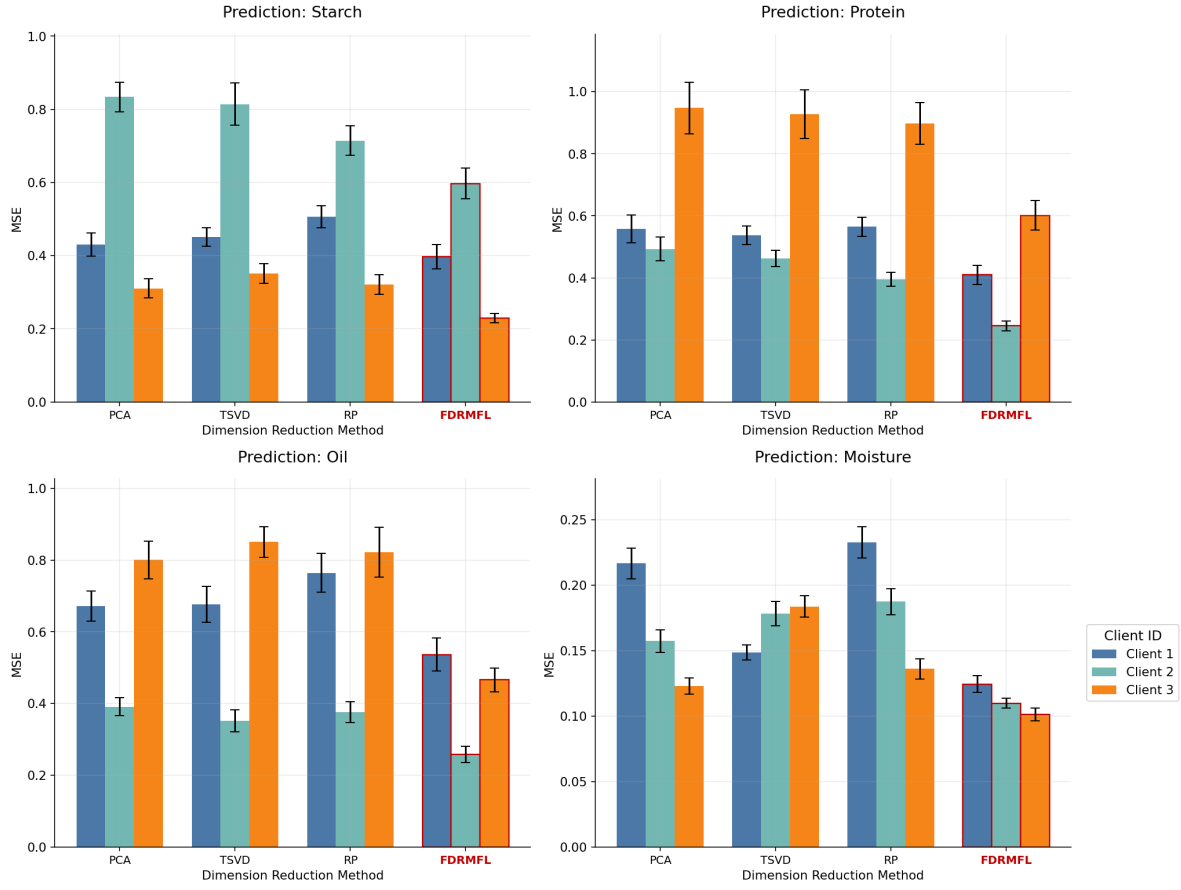


Fig. 6: Visualization of the comparison of prediction MSE by various methods under the corn dataset

Tables 3, 4 and Figures 5, 6), the bars for FDRMFL remain consistently shortest with uniform heights, visually reinforcing its core advantages of high accuracy and high stability. Taken together, these results show that FDRMFL reliably and stably outperforms traditional dimensional-reduction baselines in practical federated multimodal regression.

#### 4. Conclusions

This study focuses on the feature extraction problem in multi-modal data regression and has achieved breakthrough progress. It specifically addresses three core challenges in real-world scenarios: limited and non-independent and identically distributed (non-IID) data, effective extraction and fusion of multi-modal information, and susceptibility to catastrophic forgetting in model learning. These intertwined challenges lead to significant performance degradation of traditional feature extraction methods. To this end, this paper proposes a task-driven supervised multi-modal federated feature extraction method named FDRMFL, which integrates multi-modal information extraction and contrastive learning mechanisms and can adapt to different neural network structures as latent mapping functions for various modal data. The method enables each client to independently learn low-dimensional representations of multi-modal data

and can flexibly control the retention degree of effective response variable-related information in the low-dimensional features through parameter tuning. Combined with the dual verification of simulation experiments and real near-infrared spectroscopy (NIR) experiments, the core contributions and conclusions of this study are as follows:

Firstly, FDRMFL constructs an innovative multi constraint learning framework, which thoroughly breaks the design limitations of traditional feature extraction methods. Classical techniques such as Principal Component Analysis (PCA, aiming at variance maximization), Random Projection (RP, based on random mapping), and Truncated Singular Value Decomposition (TSVD, focusing on low-rank approximation) all take the optimization of data's own features as the core goal. In contrast, FDRMFL uses Mean Squared Error (MSE) loss as the core to ensure regression accuracy, and introduces three regularization constraints to form a synergistic effect mechanism: the mutual information preservation constraint ensures the retention of task-related information in the extracted features; the symmetric Kullback-Leibler (KL) divergence constraint realizes the extraction, fusion and alignment of multi-modal features at the distribution level; and the inter-model contrastive constraint effectively mitigates representation drift and catastrophic forgetting



in federated non-IID scenarios. This "core loss + multi-constraint synergy" design fundamentally changes the defect of traditional methods that "perform modal-independent extraction and separate downstream tasks", ensuring that the feature extraction process always centers on improving the performance of downstream regression tasks.

Secondly, extensive experimental results from simulations and real-world data analysis demonstrate that the proposed FDRMFL achieves more significant performance improvement on downstream regression tasks compared with classical feature extraction techniques. On the simulation dataset containing three nonlinear connection functions, FDRMFL achieves the lowest Mean Squared Error (MSE) in all 9 "client-connection function" combinations, with a relative performance improvement of 15.2%–52.1% compared with the second-best baseline method. More notably, its MSE fluctuation range (0.3191–0.9708) is significantly smaller than that of TSVD (0.4530–1.7937) and PCA (0.4173–0.5985), fully proving its strong stability in non-IID data scenarios. On two real near-infrared datasets (Tecator meat and Eigenvector corn), FDRMFL further verifies its industrial practical value: in the prediction tasks of 7 key chemical components (including protein, fat, moisture, starch, oil, etc.), its performance consistently outperforms all baseline methods even in the face of client-side sample distribution differences. Specifically, in the corn oil prediction task, FDRMFL reduces the MSE by 45.2% compared with TSVD on Client 3; in the meat fat prediction task, its relative performance improvement reaches 66.8% compared with PCA on Client 1. These results confirm that the constraint design of FDRMFL can effectively solve the core problems of multi-modal federated feature extraction in real data.

Finally, this study highlights the great application potential of task-driven feature extraction in federated learning. The meat and corn near-infrared datasets correspond to typical industrial scenarios such as food quality inspection and agricultural product component analysis, where there are universal rigid demands for data privacy protection and distributed collection. FDRMFL can complete high-precision and high-stability feature extraction and regression tasks locally on the client side without centralizing sensitive spectral data, providing a practical solution that balances privacy security and prediction performance for such fields. Compared with the triple dilemma of traditional methods that struggle to balance dimensionality reduction efficiency, task relevance and cross-client consistency, FDRMFL achieves the organic unification of the three through multi-constraint collaborative design.

Despite the excellent performance of FDRMFL, there are four main directions for expansion: first, the current method is mainly adapted to the three-modal scenario of "image-text-vector" and the dual-modal scenario of "spectrum-scalar"; in the future, it can be extended to more complex modal types such as sensor time-series data and audio signals, and the alignment constraints can be optimized for modal heterogeneity scenarios such as mixed discrete and continuous features. Second, the existing scheme assumes that the client

participation status is fixed during training; for dynamic federated scenarios where clients join or exit dynamically, the contrastive constraints need to be enhanced to adapt to intermittent global model updates. Third, the current model has not been in-depth designed in terms of privacy protection; in subsequent research, blockchain technology or differential privacy mechanisms can be introduced to strengthen privacy protection capabilities. Fourth, FDRMFL has not yet adapted to streaming data scenarios; in the future, continuous learning technology can be integrated to realize real-time feature extraction and regression of streaming data.

## References

- [1] Arsigny, V., Fillard, P., Pennec, X., Ayache, N., 2007. Geometric means in a novel vector space structure on symmetric positive-definite matrices. *SIAM journal on matrix analysis and applications* 29, 328–347.
- [2] Bair, E., Hastie, T., Paul, D., Tibshirani, R., 2006. Prediction by supervised principal components. *Journal of the American Statistical Association* 101, 119–137.
- [3] Baltrušaitis, T., Ahuja, C., Morency, L., 2019. Multimodal machine learning: A survey and taxonomy. *IEEE Transactions on Pattern Analysis and Machine Intelligence* 41, 423–443.
- [4] Billera, L.J., Holmes, S.P., Vogtmann, K., 2001. Geometry of the space of phylogenetic trees. *Advances in Applied Mathematics* 27, 733–767.
- [5] Bingham, E., Mannila, H., 2001. Random projection in dimensionality reduction: Applications to image and text data, in: *Proceedings of the 7th ACM SIGKDD International Conference on Knowledge Discovery and Data Mining*, ACM. pp. 245–250.
- [6] Daradkeh, Y.I., Gorokhovatskyi, V., Tvoroshenko, I., Zeghid, M., 2022. Tools for fast metric data search in structural methods for image classification. *IEEE Access* 10, 124738–124746.
- [7] Dey, T.K., Wang, Y., 2022. *Computational topology for data analysis*. Cambridge University Press.
- [8] Dryden, I.L., Koloydenko, A., Zhou, D., 2009. Non-euclidean statistics for covariance matrices, with applications to diffusion tensor imaging. *The Annals of Applied Statistics*, 1102–1123.
- [9] Dubey, P., Müller, H.G., 2022. Modeling time-varying random objects and dynamic networks. *Journal of the American Statistical Association* 117, 2252–2267.
- [10] Faraway, J.J., 2014. Regression for non-euclidean data using distance matrices. *Journal of Applied Statistics* 41, 2342–2357.
- [11] Halko, N., Martinsson, P.G., Tropp, J.A., 2011. Finding structure with randomness: Probabilistic algorithms for constructing approximate matrix decompositions. *SIAM Review* 53, 217–288.
- [12] Hein, M., 2009. Robust nonparametric regression with metric-space valued output. *Advances in neural information processing systems* 22.
- [13] Higgins, I., Matthey, L., Pal, A., Burgess, C., Glorot, X., Botvinick, M., Mohamed, S., Lerchner, A., 2017. beta-vae: Learning basic visual concepts with a constrained variational framework, in: *International Conference on Learning Representations (ICLR)*.
- [14] Hossin, M., Sulaiman, M.N., 2015. A review on evaluation metrics for data classification evaluations. *International journal of data mining & knowledge management process* 5, 1.
- [15] Kairouz, P., McMahan, H.B., Avent, B., Bellet, A., Bennis, M., et al., 2021. Advances and open problems in federated learning. *Foundations and Trends in Machine Learning* 14, 1–210.
- [16] Karacam, E., Mio, W., Okutan, O.B., 2025. Observable covariance and principal observable analysis for data on metric spaces. *arXiv preprint arXiv:2506.04003*.
- [17] Karimireddy, S.P., Kale, S., Mohri, M., Reddi, S.J., Stich, S.U., Suresh, A.T., 2020. Scaffold: Stochastic controlled averaging for federated learning, in: *Proceedings of the 37th International Conference on Machine Learning (ICML)*, PMLR. pp. 5132–5143.

- [18] Kirkpatrick, J., Pascanu, R., Rabinowitz, N.C., et al., 2017. Overcoming catastrophic forgetting in neural networks. *Proceedings of the National Academy of Sciences (PNAS)* 114, 3521–3526.
- [19] Li, T., Sahu, A.K., Zaheer, M., Sanjabi, M., Talwalkar, A., Smith, V., 2020. Federated optimization in heterogeneous networks, in: *Proceedings of the 2nd Conference on Machine Learning and Systems (MLSys)*.
- [20] Lin, Y.B., Lei, J., Bansal, M., Bertasius, G., 2022. Eclipse: Efficient long-range video retrieval using sight and sound, in: *European Conference on Computer Vision*, Springer. pp. 413–430.
- [21] Marron, J.S., Dryden, I.L., 2021. *Object oriented data analysis*. Chapman and Hall/CRC.
- [22] McMahan, H.B., Moore, E., Ramage, D., Hampson, S., Aguera y Arcas, B., 2017. Communication-efficient learning of deep networks from decentralized data, in: *Proceedings of the 20th International Conference on Artificial Intelligence and Statistics (AISTATS)*, PMLR. pp. 1273–1282.
- [23] Muscat, J., 2024. *Functional analysis: an introduction to metric spaces, Hilbert spaces, and Banach algebras*. Springer Nature.
- [24] van den Oord, A., Li, Y., Vinyals, O., 2018. Representation learning with contrastive predictive coding. URL: <https://arxiv.org/abs/1807.03748>, arXiv:1807.03748.
- [25] Schiebinger, G., Shu, J., Tabaka, M., Cleary, B., Subramanian, V., Solomon, A., Gould, J., Liu, S., Lin, S., Berube, P., et al., 2019. Optimal-transport analysis of single-cell gene expression identifies developmental trajectories in reprogramming. *Cell* 176, 928–943.
- [26] Song, J., Zheng, J., Li, P., Lu, X., Zhu, G., Shen, P., 2021. An effective multimodal image fusion method using mri and pet for alzheimer’s disease diagnosis. *Frontiers in digital health* 3, 637386.
- [27] Wen, P., Li, Y., Chen, S., Zhao, S., 2021. Remaining useful life prediction of iiot-enabled complex industrial systems with hybrid fusion of multiple information sources. *IEEE Internet of Things Journal* 8, 9045–9058.
- [28] Yuan, Y., Zhu, H., Lin, W., Marron, J.S., 2012. Local polynomial regression for symmetric positive definite matrices. *Journal of the Royal Statistical Society Series B: Statistical Methodology* 74, 697–719.